The University of Sydney

Department of Civil Engineering
Sydney NSW 2006
AUSTRALIA

http://www.civil.usyd.edu.au/

Environmental Fluids/Wind Group

Prediction of maximum wave-induced liquefaction in porous seabed using Multi-Artificial Neural Network model

Research Report No R854

Fred Cha, BE MPhil
Dong-Sheng Jeng, BE ME PhD
Michael Blumenstein, BE PhD
Hong Zhang, BE PhD

November 2005

The University of Sydney

Department of Civil Engineering
Environmental Fluids/Wind Group
http://www.civil.usyd.edu.au/

Prediction of maximum wave-induced liquefaction in porous seabed using Multi-Artificial Neural Network model

Research Report No R854

Fred Cha, BE MPhil
Dong-Sheng Jeng, BE ME PhD
Michael Blumenstein, BE PhD
Hong Zhang, BE PhD

November 2005

Abstract:
In the last decades, considerable efforts have been devoted to the phenomenon of wave-induced liquefactions, because it is one of the most important factors for analysing the seabed and designing marine structures. Although numerous studies of wave-induced liquefaction have been carried out, comparatively little is known about the impact of liquefaction on marine structures. Furthermore, most previous researches have focused on complicated mathematical theories and some laboratory work. In the present study, a data dependent approach for the prediction of the wave-induced liquefaction depth in a porous seabed is proposed, based on a multi-artificial neural network (MANN) method. Numerical results indicate that the MANN model can provide an accurate prediction of the wave-induced maximum liquefaction depth with 10% of the original database. This study demonstrates the capacity of the proposed MANN model and provides coastal engineers with another effective tool to analyse the stability of the marine sediment.

Keywords:
Wave-induced liquefaction, Artificial neural networks, Multi-artificial neural network.

Copyright Notice

Department of Civil Engineering, Research Report R854
Three-Dimensional Model for Wave-Seabed Interaction around the Head of a Breakwater

d.jeng@civil.usyd.edu.au,

Published by:
Department of Civil Engineering
The University of Sydney
Sydney NSW 2006
AUSTRALIA

November 2005

This report and other Research Reports published by The Department of Civil Engineering are available on the Internet:

http://www.civil.usyd.edu.au

Contents

1 Introduction

Most marine structures such as breakwaters and seawalls, have been used for the protection of coastal communities against natural disasters like flooding or erosion. Design of coastal structures against the wave loading has been intensive studied and improved in the past. However, the damage of such structures still occurs due to the failure of foundation around the structures. Wave-induced seabed liquefaction, which has been recognised as the cluprit of foundation failure, has been of profound interest to coastal and geotechincal engineers recently [10].

Since the 1970's, numerous investigations for wave-induced liquefaction have been carried out. Bjerrum [1] was possibly the first person who recognised and analysed wave-induced liquefaction occurring in saturated seabed sediments in connection with foundation design in the North sea. Later, Ishiara and Yamazaki [8] suggested a methodology of evaluating the magnitude of cyclic stress and wave-induced liquefaction on the basis of storm parameters, which is based on the theoretical solution of Yamamoto *et al.* [23]. Zen *et al.* [24] proposed that wave-induced liquefaction of foundations, with its subsequent slip circle failure, was one of the possible causes of the collapse of structures. Their results indicated that liquefaction might be induced by ocean waves only under the condition that the pore pressure dissipation or redistribution was restricted by the existence of layers with low permeability. Later, Taotsos *et al.* [21] evaluated pore pressure generation and liquefaction potential in the seabed floor due to cyclic wave action using a numerical model. Their results concluded that the soil permeability had a very significant influence on pore-water pressure generation and liquefaction because high permeability prevented the development of excess pore-water pressure. Zen and Yamazaki [26], using a finite difference method, investigated the mechanism of the wave-induced liquefaction and densification in a permeable seabed. From the results presented, they

concluded that the liquefaction and densification occurred alternately in the seabed even in one period of the wave loading. Most recently, the authors [13, 27] established an integrated three-dimensional model, incorporating a wave model and soil model, to investigate the wave-induced liquefaction potential in the Gold Coast region in Australia. Both non-breaking and breaking waves were considered in their model.

Recently, artificial neural networks (ANNs) have found extensive utilisation in solving many complex real-world engineering problems, such as the prediction of rainfall intensity using ANN models [5], the prediction of the environmental properties of the output stream from a wastewater treatment plant using ANNs [7], tide-forecasting using ANNs[15, 16] , and the prediction of the settlement of shallow foundations on cohesionless soils [17].

For the liquefaction consideration, ANN models have been applied to the prediction of seismic liquefaction potential by using a back-propagation neural network [6]. Juang and Chen [14] also predicted seismic liquefaction potential from cone penetration field test data. Cha [4] and Jeng [12] were possibly the first to apply ANNs to the prediction of wave-induced liquefaction in a porous seabed. Their research demonstrated the capability of ANN models for the prediction of the maximum wave-induced liquefaction depth within various wave and soil conditions. However, only a single artificial neural network(SANN) model was introduced in their study, which had unclear predictions at particular ranges of liquefaction depth.

The goal of this study is to develop a multi-artificial neural network model to predict the wave-induced liquefaction potential, especially the maximum liquefaction depth. Using the results obtained from the existing theories developed by the author [3]. Subsequently, a MANN model will be investigated for the improvement of the accuracy of the existing SANN model. Finally, a series of numerical experiments will be conducted to demonstrate the capability of the proposed MANN model.

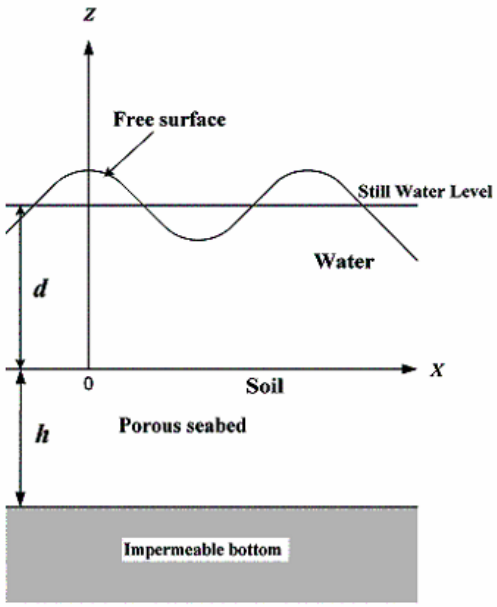

Figure 1: Definition of wave-seabed interaction.

2 Theoretical Formulations

2.1 Wave-induced soil response

In this study, we consider an ocean wave propagating over a porous seabed of finite thickness. The definition of the problem is illustrated in Figure 1. The porous seabed is treated as hydraulically isotropic with the same permeability in all directions. Zienkiewicz *et al.* [28] presented a general set of governing equations, which describe the behaviour of a linear elastic porous solid under dynamic conditions. These equations are summarised in a tensor form as below

$$\sigma_{ij,j} = \rho\ddot{u}_i + \rho_f\ddot{w}_i, \tag{1}$$

$$-p_{,i} = \rho_f\ddot{u}_i + \frac{\rho_f}{n}\ddot{w}_i + \frac{\rho_f g}{k_z}\dot{w}_i, \tag{2}$$

$$\dot{\varepsilon}_{ii} + \dot{w}_{i,i} = -\frac{n}{K_f}\dot{p}, \tag{3}$$

where p is the pore pressure in excess of hydrostatic, n is the porosity, ρ is the combined soil density; ρ_f is the fluid density, u and w are the displacements of solid and relative displacements of solid and pore fluid. $1/K_f$ is the compressibility of pore-fluid, which is defined by

$$\frac{1}{K_f} = \frac{1}{2\times 10^9} + \frac{1-S}{P_{wo}} \tag{4}$$

in which S is the degree of saturation, P_{wo} is the absolute water pressure. The definition of effective stresses, σ'_{ij}, which are assumed to control the deformation of the soil skeleton are given by the total stress (σ_{ij}) and pore pressure (p) as,

$$\sigma_{ij} = \sigma'_{ij} - \delta_{ij}p, \tag{5}$$

where δ_{ij} is the Delta denotation. It is noted that the tensile stresses are represented as positive signs, while pore pressure is compression positive in this study.

Therefore, the equation of force balance, equation (1) becomes

$$\sigma'_{ij,j} = \delta_{ij}p_{,i} + \rho\ddot{u}_i + \rho_f\ \ddot{w}_i. \tag{6}$$

To obtain the wave-induced pore pressure, soil and fluid displacements involved in (1)-(3), appropriate boundary conditions are required. The boundary conditions are summarised below,

$$u = w = 0,\ p = 0\ \ as\ \ z \to -\infty \tag{7}$$

$$p = P_b,\ \sigma_z^{'} = \tau = 0 \quad at \quad z = 0 \tag{8}$$

where, P_b is the wave pressure at the seabed surface, which is given by the equation below:

$$P_b = \frac{\gamma_w H}{\cosh kd} \cos(kx - \omega t), \tag{9}$$

where H is the wave height and d is the water depth, k is the wave number, ω is wave frequency, and γ_w is the unit weight of water.

Following the procedure in Cha [3], the general solution for the soil and pore fluid displacements, to satisfy the bottom boundary condition (7), can be expressed as

$$\bar{U}_x = a_1 e^{\lambda_1 \bar{z}} + a_3 e^{\lambda_2 \bar{z}} + a_5 e^{\lambda_3 \bar{z}} \tag{10}$$

$$\bar{U}_z = a_1 b_1 e^{\lambda_1 \bar{z}} + a_3 b_3 e^{\lambda_2 \bar{z}} + a_5 b_5 e^{\lambda_3 \bar{z}} \tag{11}$$

$$\bar{W}_x = a_1 c_1 e^{\lambda_1 \bar{z}} + a_3 c_3 e^{\lambda_2 \bar{z}} + a_5 c_5 e^{\lambda_3 \bar{z}} \tag{12}$$

$$\bar{W}_z = a_1 d_1 e^{\lambda_1 \bar{z}} + a_3 d_3 e^{\lambda_2 \bar{z}} + a_5 d_5 e^{\lambda_3 \bar{z}} \tag{13}$$

where λ_i coefficients are the roots of the characteristics equation from the couple of equation. Based on the wave-induced soil and fluid displacements, we can obtain the wave-induced pore pressure, effective stresses and shear stress. The unknown coefficients, a_i, b_i, c_i and d_i, can be solved with the boundary condition. Once we obtain coefficients, we can calculate the wave-induced soil response parameters. Detailed information of the above solution can be found in Jeng and Cha [11].

2.2 Wave-induced liquefaction

It has generally been accepted that, when the vertical effective stress vanishes, the soil will be liquefied. Under such a situation, the soil matrix loses its strength to carry any load and consequently causes seabed instability. However, the mechanisms of the wave-induced soil

liquefaction in marine sediments have not been clearly addressed in geotechnical terms at the present stage. The liquefaction is also affected by the state of soil compaction, permeability, the wave-induced cyclic stress as well as the degree of drainage.

To apply the concept of excess pore pressure to a seabed, a schematic drawing of the pore pressure and effective stress distributions is illustrated in Figure 2. The solid curves in the figure indicate the pore pressure beneath a wave trough and a wave crest. The excess pore pressure is transient in nature, because both P_b and p are oscillatory and periodical in real ocean environments. Consequently, the effective stress varies periodically in accordance with the change of the excess pore pressure. If it attains zero or a negative value at certain depths below the seabed surface, the soil skeleton will reach a liquefied state (Figure 2). Thus, the liquefaction criterion can be expressed as [9, 25]

$$-\frac{1}{3}(\gamma_s - \gamma_w)(1 + 2K_o)z + (P_b - p) \leq 0. \tag{14}$$

where K_o is the coefficient of earth pressure at rest, which is normally varied from 0.4 to 1.0 and 0.5 is commonly used for marine sediments [20].

Although other criteria of the wave-induced liquefaction have been proposed based on the concept of effective stresses [18, 22], the crition based on the concept of excess pore pressure [25, 9] was demonstrated to be a better criertion of liquefaction, comparing with the field data [9].

3 Artificial neural networks

Artificial neural networks (ANNs) are computing systems made up of a number of simple, highly interconnected processing elements, which process information by their dynamic state response to external inputs [2]. ANNs have been developed since the early 1940's,

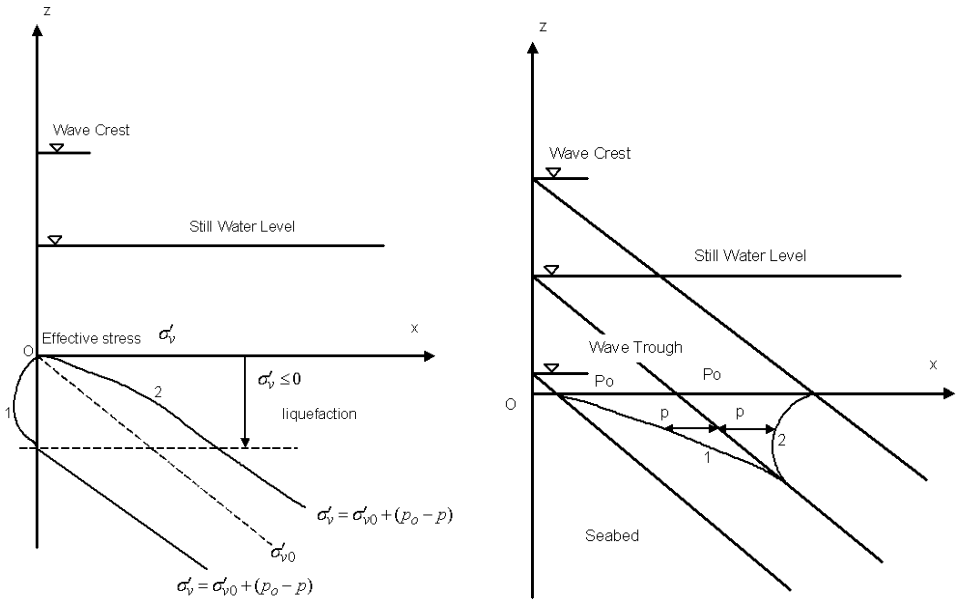

(a) Concept of excess pore pressure (b) Criterion of liquefaction

Figure 2: The concept of excess pore pressure and criterion of liquefaction (After Zen and Yamazaki [25]

they were not applied to real-world problems until the middle of the 1980's when algorithms became sophisticated enough for general applications.

Figure 3 illustrates an artificial neuron in comparison with a basic human brain neuron. It is clearly shown that artificial neurons are based on the most simplest functions of the human brain. An ANN model can be built, based on the artificial neuron (Fig 3(b)). Figure 4 shows that a typical ANN model includes an input layer, hidden layer(s) and output layer. Each layer is made up of several neurons and the layers are interconnected by sets of corresponding weights. The input layer neurons receive initial input information, after which, outputs may be obtained by using various transfer functions. In this paper, we adopted the logarithmic sigmoid transfer function is adopted, which can be expressed as

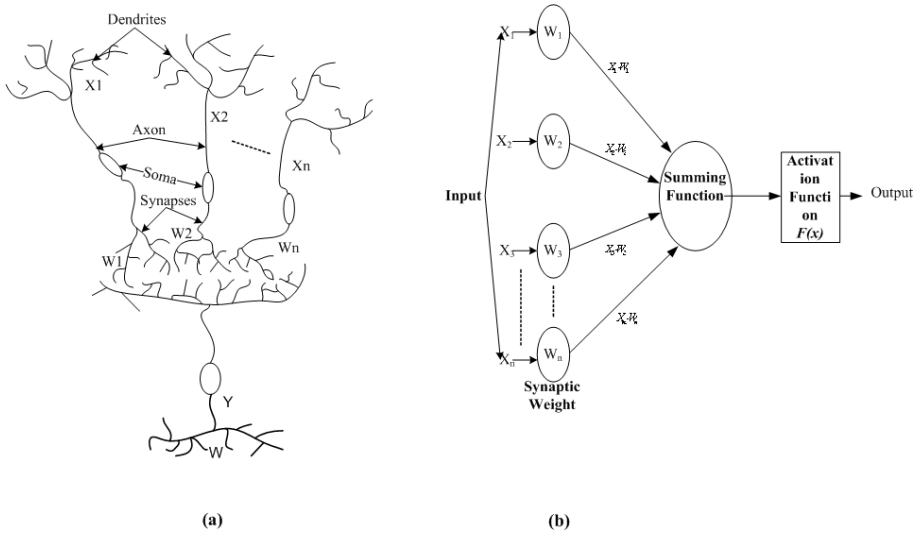

Figure 3: (a) Biological neuron from human brain. (b)Basic artificial neuron.

$$f(x) = \frac{1}{1 + e^{-x}} \tag{15}$$

In the learning procedure, which is also called training, using an appropriate data set, the interconnection weights are adjusted based on the interaction between input and output values, which is an important part of the ANN model. In this study, the back-propagation algorithm is applied. The back-propagation network is the most representative model for various applications of artificial neural networks. The back–propagation algorithm can be applied to networks that contain at least one hidden layer, and fully connected units in each layer. This configuration results in a network architecture as shown in Figure 4. The main procedure of the back-propagation network is that the error at the output layer continuously propagates backward to the input layer through the hidden layer(s) in the network to obtain the final desired response. It clearly means that the goal of this procedure is to obtain a desired output when certain inputs are given. The error function, which is used in this paper, is given as

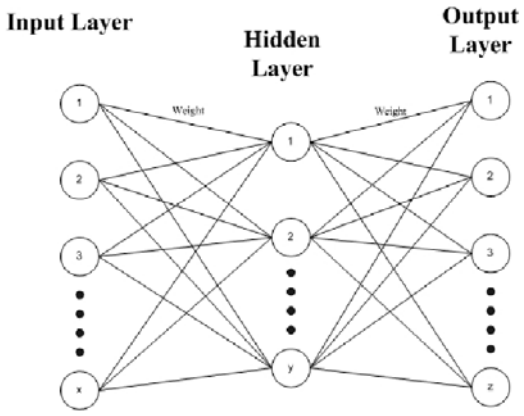

Figure 4: Typical artificial neural network model.

$$E = \frac{1}{M}\sum_{i}^{M}(D_i - O_i)^2 \tag{16}$$

where D_i and O_i are the desired and the actual output values respectively, M is the total number of training data set. Since the error is the difference between the actual output and the target output, the error produced depends on the configuration of the weights, and hence it is necessary to adjust the weights in order to minimize the error. The method of gradient descent is employed to adjust the weights. The details of the back-propagation algorithm can be found in Rumelhart [19].

3.1 ANN model for wave-induced liquefaction

Wave-induced seabed liquefaction was previously predicted by solving complicated mathematical equations. However, the existing deterministic models have been based on various assumptions, which have limited the application of the models. The ANN model does not

involve all the physical equations, that only requires reliable input data, which are obtained from previous historic, field data or numerical solutions. In this study, a database was generated from the numerical model described in section 2. The structure of the proposed ANN model, which is used in this study, is illustrated in Figure 5. A multi-layered back-propagation network with sigmoidal activation functions is used, which is the most popular scheme employed in engineering prediction or forecasting problems.

The parameters used as inputs to the ANN model are permeability (fixed value), the degree of saturation, the seabed depth, the wave period, the wave height, and the water depth. It has been reported that soil permeability is very sensitive to the occurrence of the wave-induced liquefaction potential [9]. In general, permeabilities of different soils are in different order, which make the procedure of normalisation to be difficult. After preliminary tests of ANN models, we found that inclusion of permeability cause the difficulties of convergence of the model. Thus, we have an ANN model for each case with a fixed value of soil permeability. This will make the proposed ANN model much easier to converge.

In this study, a multi-artificial neural network (MANN) is introduced, which is extends the Single-artificial neural network (SANN) developed in the author's previous study [12]. The major difference between the SANN model and the MANN model is the number of networks used. The SANN model is comprised of only one network which is used for the whole database, and the MANN is composed of various networks depending on the range of the database.

3.2 Numerical simulations

The performance of ANN models depends on the number of hidden layers, the learning factors, the number of training iterations (epochs), the weight configurations and the

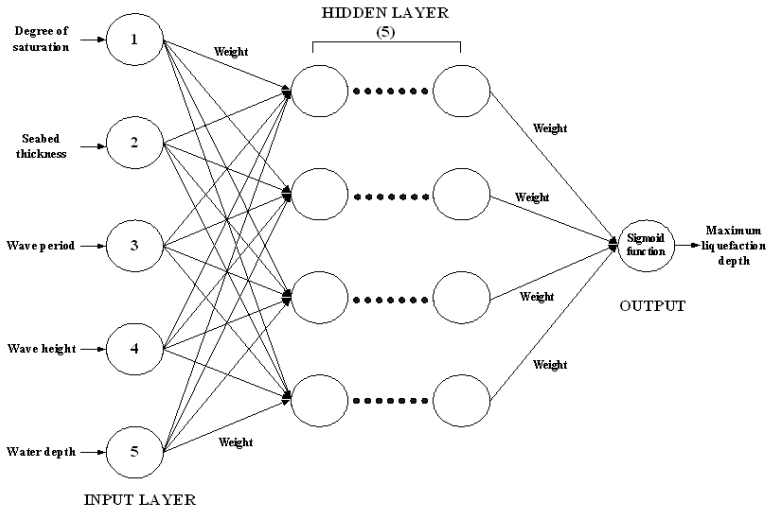

Figure 5: Architecture of the proposed ANN model for wave-induced liquefaction.

number of neurons in each layer. These factors, for this study, are tabulated in Table 1. The ANN model is established using the MATLAB ANN ToolBox environment.

The input data for the poro-elastic model, which establishes the database of the ANN model, are shown in Table 2. As seen in the table, the data set has covered most of the possible ranges of wave and soil conditions. Three different soil permeabilities , representing three different sandy seabeds (coarse and fine sand), are used in this study. The

Table 1: Structure of ANN model

Training model	
Number of input neurons	5
Number of output neurons	1
Number of hidden units	4
Number of hidden layer	5
Learning rate	0.5
Momentum factor	0.2
Epochs	9000

Table 2: Input data of theoretical model

Wave characteristics	
Wave period (T)	Varying between $5sec$ and $15sec$
Wave height (H)	Varying between $0.5m$ and $8m$
Water depth (d)	Varying between $10m$ and $50m$
Soil characteristics	
Soil permeability (K_z)	$10^{-4}, 5 \times 10^{-4}, 5 \times 10^{-6}$m/sec
Seabed thickness (h)	Varying between $10m$ to $60m$
Shear modulus (G)	10^7 N/m^2
Poisson's ratio (μ)	0.4
Porosity (n)	0.4
Degree of saturation (S)	Varying between 0.95 and 1.0

poro-elastic numerical model test results indicate that wave-induced liquefaction occurs in numerous cases. The whole database contains approximately 50,000 cases of wave-induced maximum liquefaction depth.

In this case study, we chose a data set of size 20,000 (approximately) of maximum liquefaction depth from the poro-elastic numerical model. From this database, 80% of the data is used for the training procedure, and the remaining data is for model verification.

3.2.1 Data acquisition

In this study, a database including wave, soil parameters and maximum liquefaction depth is generated from a numerical model based on various parameters (Table 2). However, the ANN model had a limitation of input and output values between 0 and 1 or -1 and 1, due to the ANN's activation functions, which is a main aspect of the model. Therefore, the input and output values are converted to suit this range. For example, 60 m for seabed thickness is converted to 0.6 hundred metres. It is a clearly shown that the ANNs required appropriate data acquisition and preprocessing steps to build a database for training, even if good quality data was collected.

3.2.2 Single-artificial neural network model (SANN)

The advantages of the single-network model [4], were its simplicity and limited time consumption. The test results for prediction of the maximum liquefaction depth and the training procedure using the proposed SANN model are presented in Figures 6 – 8.

Figure 6(a) illustrates the convergence of the training procedure. It is clearly shown that the training error is less than 10^{-3}, which is based on (16). It implies that the SANN weight configuration can be used to forecast the maximum liquefaction depth with a good accuracy. Figure 6(b) represents the prediction of the maximum liquefaction depth (Z_L) using the ANN model versus the poro-elastic numerical maximum liquefaction depth (Z_L). As seen in this figure, the prediction of maximum liquefaction agrees with the numerical calculation data overall.

However, as shown in Figures 6–8, there is significant disagreement between the SANN model and the original database near the origin (i.e., no liquefaction). This implies that a single-network model may not be able to predict the maximum liquefaction depth if it is either small or zero.

3.2.3 Multi-artificial neural network model (MANN)

The occurrence of wave-induced liquefaction depends on soil and wave parameters. However, as shown in Figures (6)–(8), SANN model fails to predict values near the zero liquefaction and over 3 m liquefaction depth range. Therefore, MANN model is applied to deal with three different ranges, from 0 to 1 m, 1 to 3 m and 3 to 5 m, with three different networks. Figure 9 illustrates the construction of the MANN model. These ranges are based on preliminary tests, and finalise it to be the best option for this problem. It has a similar training procedure to the SANN model, but the data used for training is divided into 3 different training databases (Figure 10).

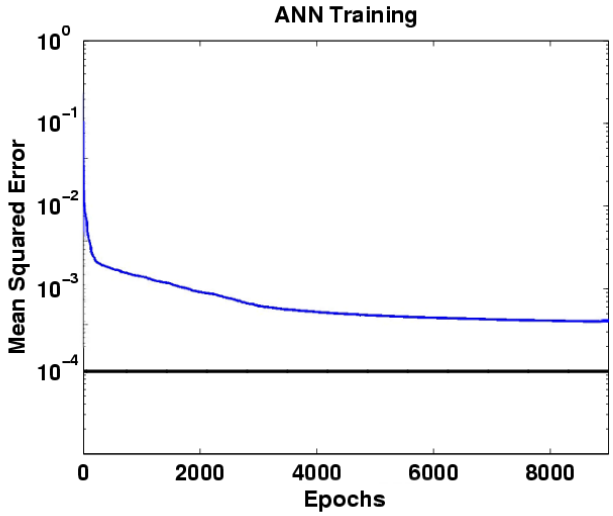

(a) Convergence of training data

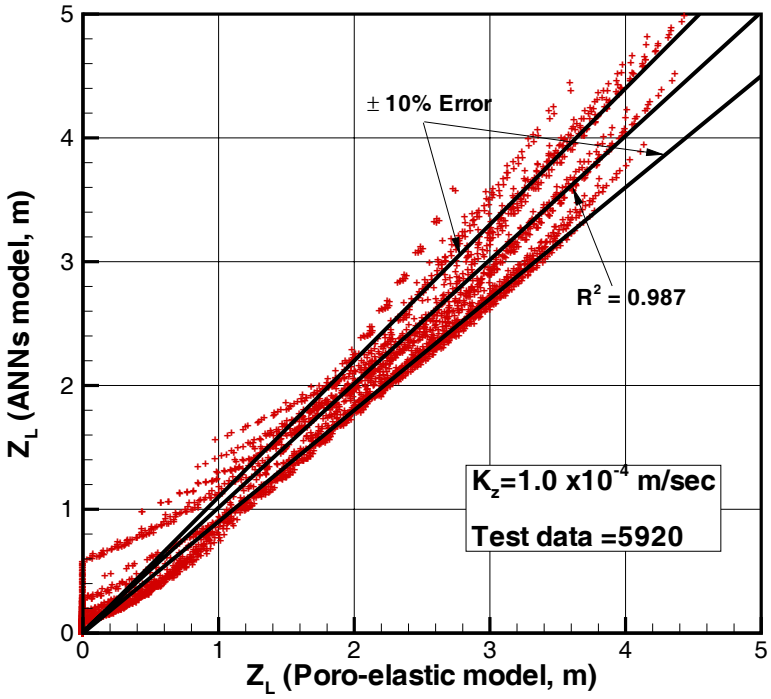

(b) Prediction of the SANN model versus the poro-elastic model

Figure 6: (a) Convergence of training data and (b) comparison of the the wave-induced maximum liquefaction depth by the SANN model versus the poro-elastic model ($K_z = 10^{-4}$ m/sec).

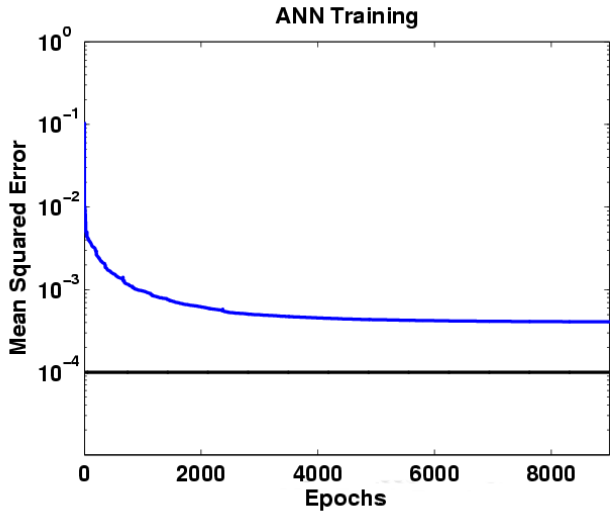

(a) Convergence of training data

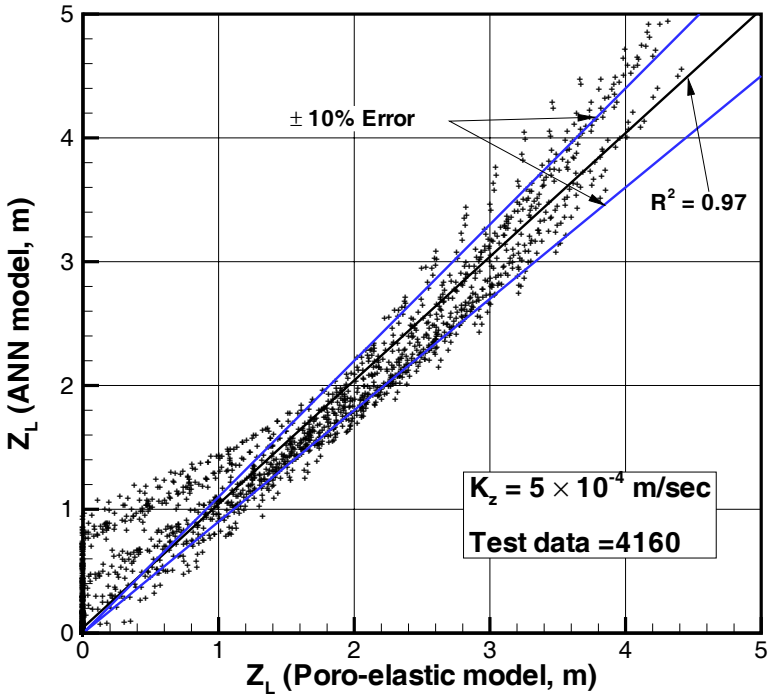

(b) Prediction of the SANN model versus the poro-elastic model

Figure 7: (a) Convergence of training data and (b) comparison of the the wave-induced maximum liquefaction depth by the SANN model versus the poro-elastic model ($K_z = 5 \times 10^{-4}$ m/sec).

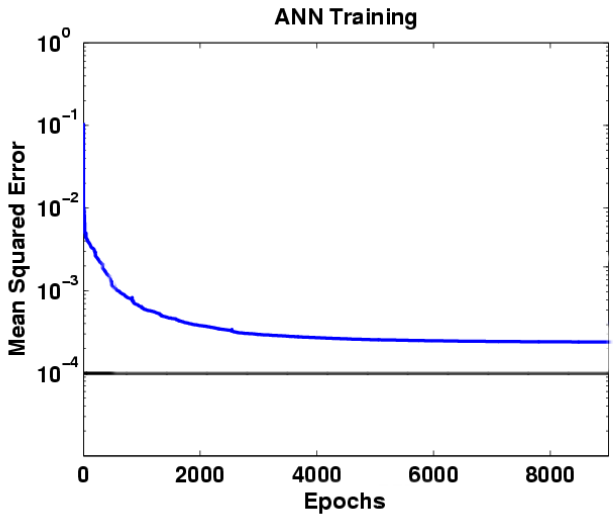

(a) Convergence of training data

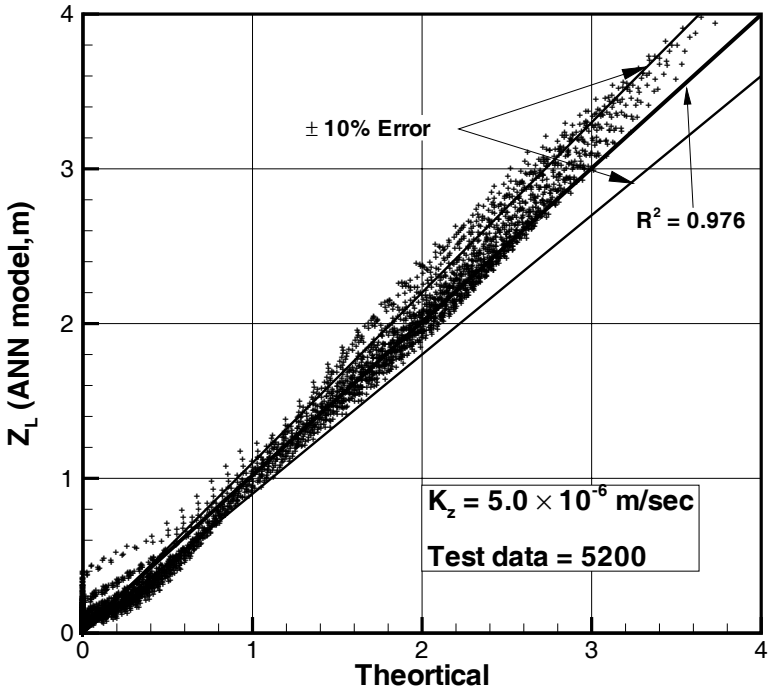

(b) Prediction of the SANN model versus the poro-elastic model

Figure 8: (a) Convergence of training data and (b) comparison of the the wave-induced maximum liquefaction depth by the SANN model versus the poro-elastic model ($K_z = 5 \times 10^{-6}$ m/sec).

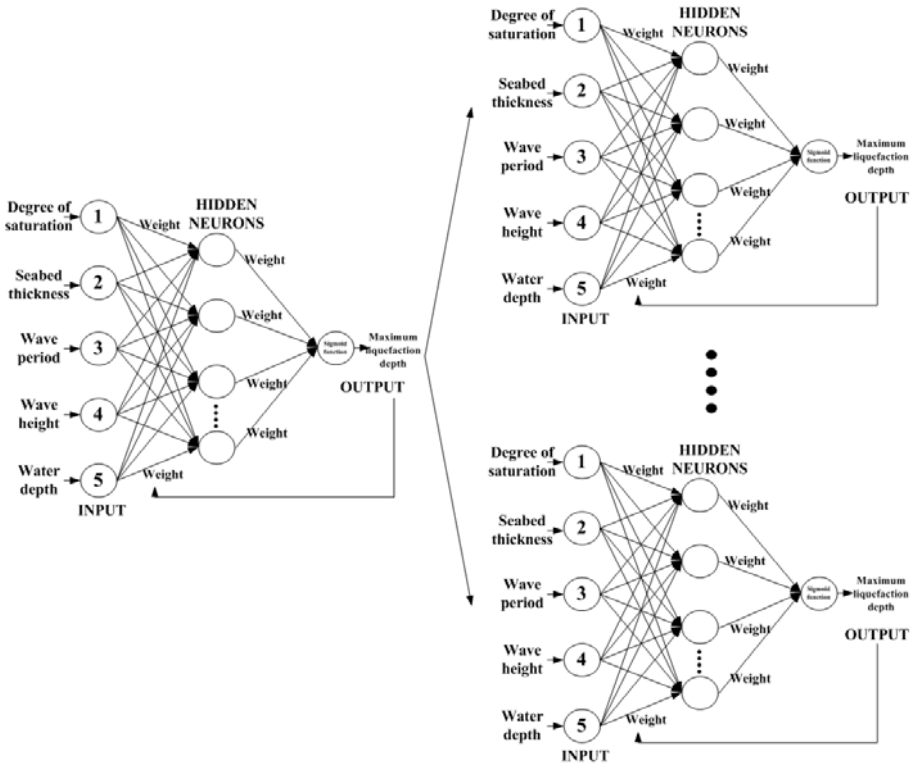

Figure 9: Architecture of MANN model

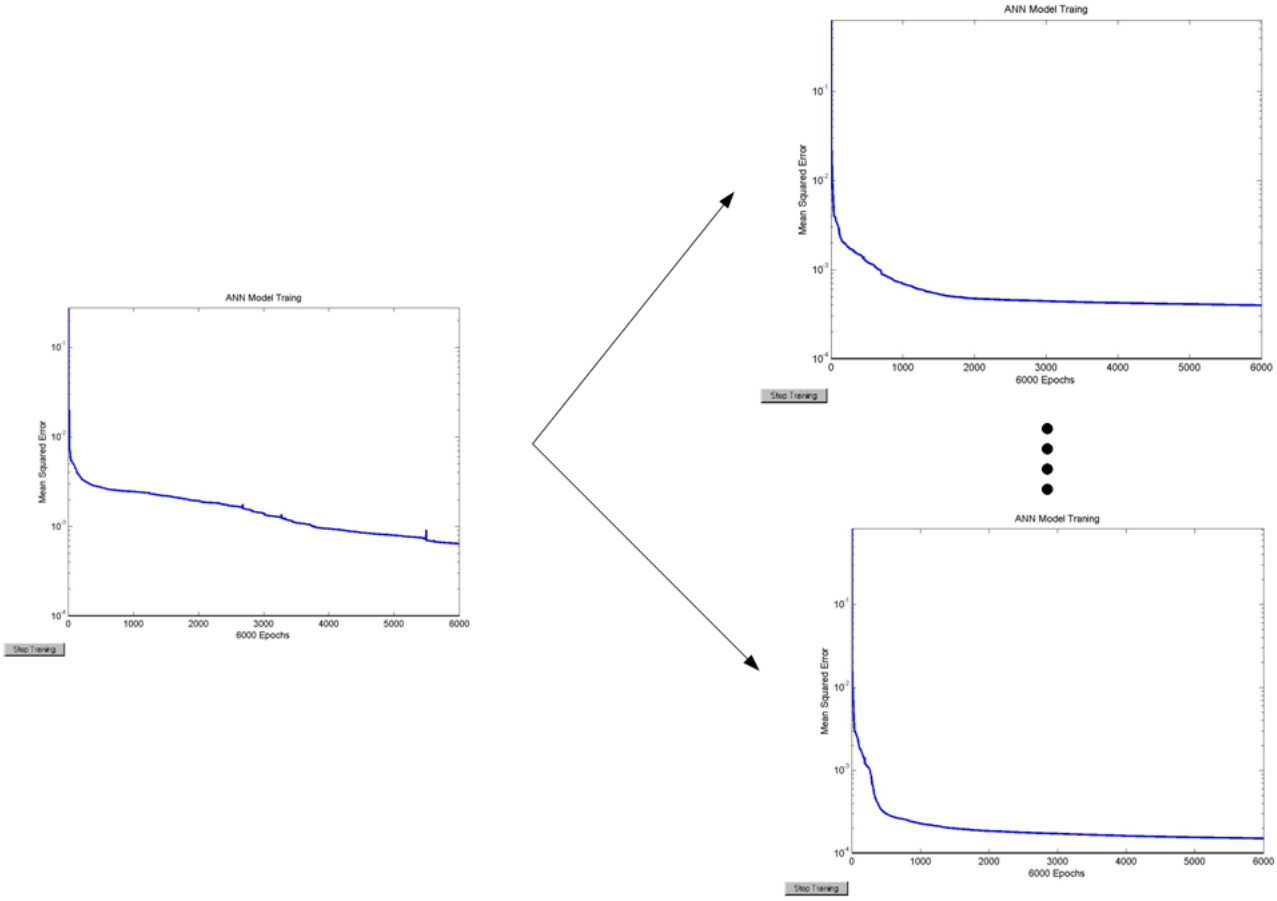

Figure 10: Convergence of MANN model training data

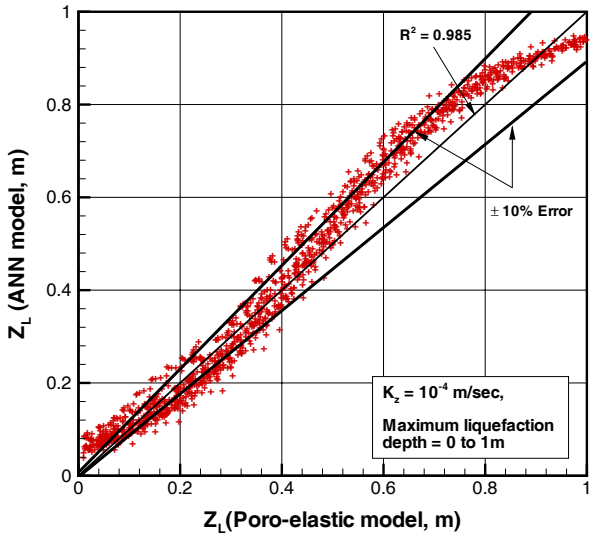

Figure 11: (a) Comparison of the the wave-induced maximum liquefaction depth by the MANN model versus poro-elastic model. Maximum liquefaction depth between 0 to 1 m ($K_z = 10^{-4}$ m/sec)

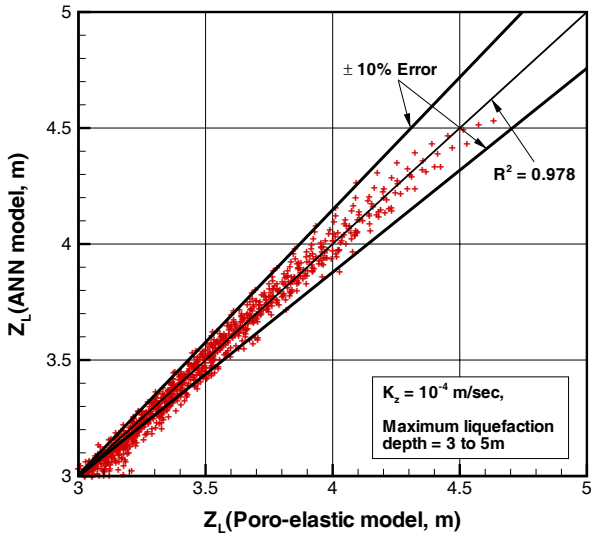

Figure 11: (b) Comparison of the the wave-induced maximum liquefaction depth by the MANN model versus poro-elastic model. Maximum liquefaction depth between 1 to 3 m ($K_z = 10^{-4}$ m/sec)

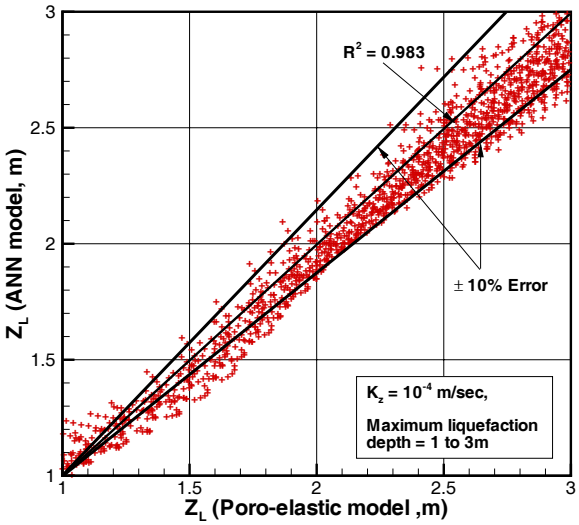

Figure 11: (c) Comparison of the the wave-induced maximum liquefaction depth by the MANN model versus poro-elastic model. Maximum liquefaction depth between 3 to 5 m. ($K_z = 10^{-4}$ m/sec)

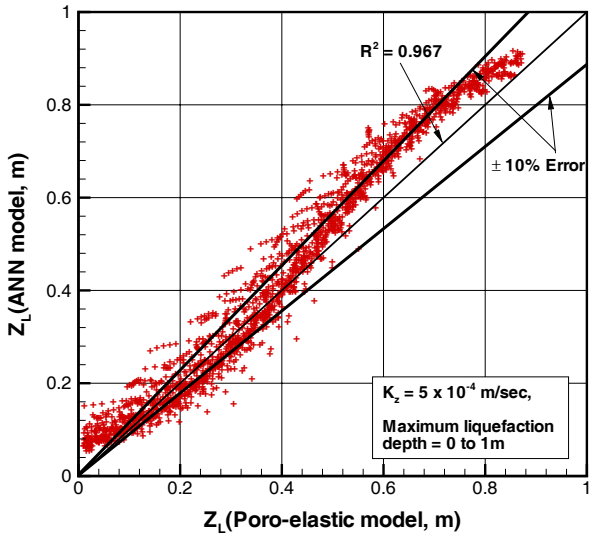

Figure 12: (a) Comparison of the the wave-induced maximum liquefaction depth by the MANN model versus poro-elastic model. Maximum liquefaction depth between 0 to 1 m ($K_z = 5 \times 10^{-4}$ m/sec)

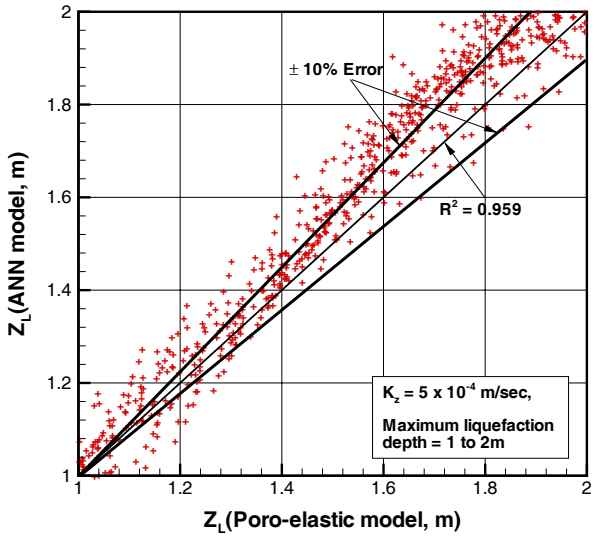

Figure 12: (b) Comparison of the the wave-induced maximum liquefaction depth by the MANN model versus poro-elastic model. Maximum liquefaction depth between 1 to 3 m ($K_z = 5 \times 10^{-4}$ m/sec)

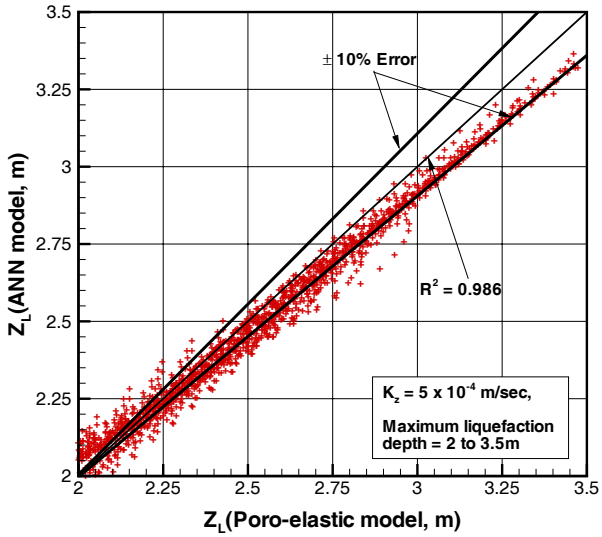

Figure 12: (c) Comparison of the the wave-induced maximum liquefaction depth by the MANN model versus poro-elastic model. Maximum liquefaction depth between 3 to 5 m ($K_z = 5 \times 10^{-4}$ m/sec)

To apply the MANN, the ANN model for the range of 1-3 m will be used for the testing database first, because most cases will locate in the range. If the results obtained from the model of 1- 3 m is out of the range, we can use another two models to further confirm the results with new range of maximum liquefaction depth.

Figure 11 clearly shows that each range of maximum liquefaction depth of the MANN predicted results agrees with the numerical calculation depths. It is obvious that maximum liquefaction depth ranges between 0 to 1 m and 3 to 5 m have a good agreement between the MANN and poro-elastic modelsl. It also shows that the correlation of the MANN model and the poro-elastic model is over 97% for all ranges. These figures illustrate that difference of the predictions of maximum depths are within the $\pm 10\%$ range, which is acceptable for an engineering application. The results indicate that if we can control the range of data in each case, the accuracy for the ANN model can be improved. In other words, if the weights for each case can be optimised, the accuracy of prediction will be dramatically increased. Similar trends for other ranges of K_z have been observed in Figures 11-12.

4 Conclusions

In this paper, we established and compared SANN and MANN models, and applied these models to the prediction of the wave-induced liquefaction potential in a porous seabed. ANNs are still fresh and an un-explored area in engineering. The results in this paper clearly show that the MANN model provides good accuracy in the prediction of the wave-induced maximum liquefaction depth. It also shows that ANNs can be a powerful engineering tool in future research. Unlike conventional engineering mechanics approaches, ANN models do not require a complicated mathematical procedure. Numerical examples have demonstrated that MANN model is applicable for the prediction of the wave-induced maximum liquefaction depth with reasonable accuracy.

Acknowledgement

The authors thank the support from a Griffith University Research and Development Grant (GURD, 2004).

References

[1] Bjerrum J. Geotechnical problem involved in foundations of structures in the North Sea. Géotechnique, 1973;23(3):319-358

[2] Caudill M. Neural Networks primer, Part I. AI expert, 1987: 46-52

[3] Cha DH. Mechanism of Ocean Waves Propagating over a Porous Seabed. MPhill Thesis. Griffith University, Australia, 2003.

[4] Cha DH, Jeng DS, Blumenstein M. Assessment of wave-induced liquefaction in a porous seabed: Application of an ANN model. Asian Journal of Information Technology, 2004;3(5), 386-399.

[5] French NM, Witol F, Krajewski FW, Cuykendallb RR. Rainfall forecasting in space and time using a neural network. Journal of Hydrology, 1992;137:1-31.

[6] Goh ATC. Seismic liquefaction potential assessed by neural networks. Journal of Geotechnical Engineering, ASCE, 1995;120:1467-1480.

[7] Gontarski CA, Rodrigues PR, Mori M, Prenem LF. Simulation of an industrial wastewater treatment plant using artificial neural networks. Computers and Chemical Engineering, 2000;24:1719-1723.

[8] Ishihara K, Yamazaki A. Analysis of wave-induced liquefaction in seabed deposit sand. Soil and Foundation, 1984;24(3):85-100.

[9] Jeng DS. Wave-induced seabed instability in front of a breakwater. Ocean Engineering, 1997;24(10):887-917.

[10] Jeng DS. Wave-induced seafloor dynamics. Applied Mechanics Review, 2004;56(4):407-429.

[11] Jeng DS, Cha DH. Effects of dynamic soil behaviour and wave non-linearity on the wave-induced pore pressure and effective stresses in porous seabed. Ocean Engineering, 2003;30(16):2065-2089.

[12] Jeng DS, Cha DH, Blumenstein M. Neural Network model for the prediction of the wave-induced liquefaction potential in a porous seabed. Ocean Engineering, 2004;31(17-18):2073-2086.

[13] Jeng DS, Zhang H. An integrated three-dimensional model for wave-induced pore pressure and effective stresses in a porous seabed. II: Breaking waves. Ocean Engineering, 2005;32(16):1950-1967.

[14] Juang CH, Chen CJ. CPT-based liquefaction evaluation using neural network. Journal of Coumputer-Aided Civil Infrastructure Engineering, 1999;14:221-229.

[15] Lee TL. Jeng DS. Application of artificial neural networks in tide-forecasting. Ocean Engineering, 2002;29(9):1003-1022.

[16] Lee TL, Tsai CP, Jeng DS, Shieh RJ. Neural network for the prediction and supplement of tidal record in Taichung Harbor, Taiwan. Advances in Engineering Software, 2002;(33):329-338.

[17] Mohamed SK, Holger RM, Mark BJ. Predicting Settlement of Shallow Foundations using Neural Networks. Journal of Geotechnical and Geo environmental Engineering, 2002;128(9):785-793.

[18] Okusa S. Wave-induced stresses in unsaturated submarine sediments. Géotechnique, 1985;35(4):517-532.

[19] Rumelhart DE,Hinton GE, Williams RJ. Learning representations by back-propagating errors. Nature, 1986; 323:53-536.

[20] Scott RF. Principle of Soil Mechanics. Addison-Publishing. Massachussetts, 1963.

[21] Taotsos S, Georgiadis M, Damakindow A. Numerical analysis of liquefaction potential of partially drained seafloor. Coastal Engineering, 1989;13(2):117-128.

[22] Tsai CP. Wave-induced liquefaction potential in a porous seabed in front of a break-water. Ocean Engineering, 1995;22(1):1-18.

[23] Yamamoto T, Koning HL, Sellmejjer H, Hijum EV. On the response of a poro-elastic bed to water waves. Journal of Fluid Mechanics, 1978;87:193-206.

[24] Zen K, Umehara Y, Finn WDL. A case study of the wave-induced liquefaction of sand layers under damaged breakwater. Proceedings 3rd Canadian Conference on Marine Geotechnical Engineering, 1985; 505-520.

[25] Zen K, Yamazaki H. Mechanism of wave-induced liquefaction and densification in seabed. Soils and Foundations, 1990;30:90-104

[26] Zen K, Yamazaki H. Wave-induced liquefaction in a permeable seabed. Report, port and Harbour Research Institute, 1993;31(5):155-192.

[27] Zhang H, Jeng DS. An integrated three-dimensional model for wave-induced pore pressure and effective stresses in a porous seabed. I: A sloping seabed. Ocean Engineering, 2005; 32(5-6):701-729.

[28] Zienkiewicz OC, Chang CT, Bettess P. Drained, undrained, consolidating and dynamic behaviour assumption in soils. Géotechnique, 1980;30(4):385-395.